ACS Energy Letters

http://pubs.acs.org/journal/aelccp

Generating H^+ in Catholyte and OH^- in Anolyte: An Approach to Improve the Stability of Aqueous Zinc-Ion Batteries

Yuhang Dai,[#] Jinghao Li,[#] Lineng Chen, Kehan Le, Zhijun Cai, Qinyou An, Lei Zhang,* and Liqiang Mai*

Cite This: *ACS Energy Lett.* 2021, 6, 684–686

Read Online

ABSTRACT: We used bipolar membranes (BMs) as separators in aqueous zinc-ion batteries to decouple the electrolyte, which increased the H^+ concentration in the catholyte and the OH^- concentration in the anolyte when cycling starting. An ultra-long running time of ~4440 h was achieved due to the significantly enhanced H^+ insertion in the cathode and the formation of $Zn_x(OTf)_y(OH)_{2x-y}$·nH_2O protective layers on the zinc anode.

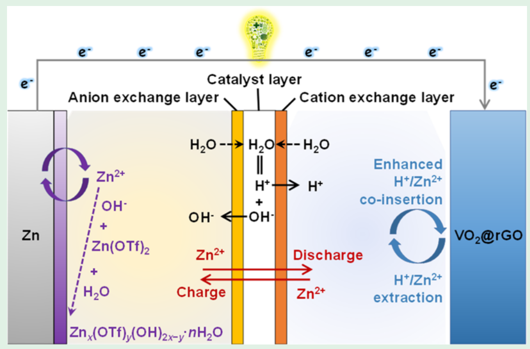

The booming global demand for large-scale energy storage, electric vehicles, and portable devices calls for energy storage devices possessing high safety, low cost, high energy density, and environmental friendliness. Aqueous zinc-ion batteries (AZIBs) meet the above requirements,[1−3] and thus interest in them has been surging in recent years. However, the poor cycling stability of AZIBs hinders their further development severely. The main challenges are to construct highly stable cathodes that can withstand divalent Zn^{2+} chemistry and solve severe zinc dendrite problems.[4]

Concerning the cathodes, the universal Zn^{2+}/H^+ co-insertion in AZIBs is discovered to cause an opposite change of lattice spacing, which enhances structural stability.[5] On the other hand, protection of the Zn anode through surface modifications shows great potential for improving batteries' stability.[6,7] Strategies that can simultaneously enhance H^+ storage and protect the Zn anode would help construct ultra-stable AZIBs but are lacking. Moreover, the pH of the electrolyte has a significant effect on a battery's cycling stability. Generally, mildly acidic or neutral aqueous electrolytes reduce Zn anode corrosion and facilitate Zn^{2+} intercalation into the cathode,[8] which improves AZIBs' cycling stability. Unlike the conventional approaches, we decouple the acidity or alkalinity of the electrolyte in situ via a bipolar membrane (BM) separator. When a constant current is applied during cycling, the BM increases the H^+ concentration in the catholyte and leads to more pronounced H^+ insertion into the cathode, while it increases the OH^- concentration in the anolyte and facilitates the formation of a $Zn_x(OTf)_y(OH)_{2x-y}$·nH_2O protective coating upon the zinc anode, which effectively suppresses the zinc dendrite formation.

Moreover, different from previous works using a BM to separate two different electrolytes,[9] we use only one kind of electrolyte while the BM separator functions as a "pump" to generate H^+ in the catholyte and OH^- in the anolyte. Modifying the separator's polarity provides an efficient and facile way to promote the leapfrog development of AZIBs.

A VO_2 nanosheets/rGO composite (VO_2@rGO) was synthesized[10] and served as cathode (Supporting Information, Figures S1 and S2). Next, CR2016 coin-type cells were assembled with VO_2@rGO as the cathode, zinc foil the anode, 3 M $Zn(OTf)_2$ aqueous solution the electrolyte, and BM and glass fiber (GF) as the separators, respectively, to investigate the electrochemical performance (the cell with bipolar membrane is denoted as BMC and that with glass fiber as GFC). We observed that the catholyte's pH was ~4.4 for GFC and 3.8 for BMC after cycling (Figure S4), revealing that the BM successfully increased the H^+ concentration in the catholyte.

Received: December 28, 2020
Accepted: January 18, 2021
Published: January 27, 2021

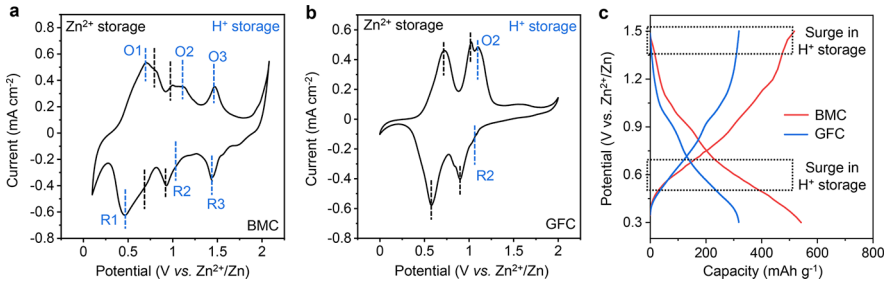

Figure 1. Cyclic voltammetry curves of (a) BMC and (b) GFC at 0.1 mV s^{-1}. (c) Galvanostatic charge/discharge curves of BMC and GFC at 100 mA g^{-1}.

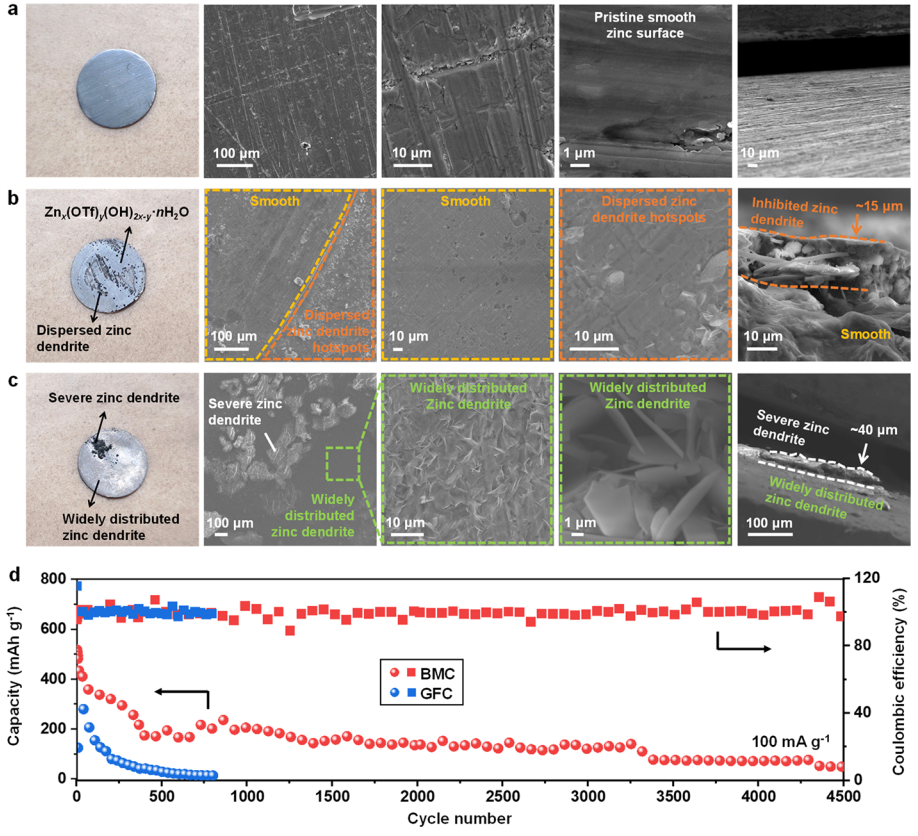

Figure 2. Optical and SEM images of zinc foil at different states: (a) pristine, (b) cycled in BMC, and (c) cycled in GFC. (d) Long-term cycle performance of BMC and GFC at 100 mA g^{-1}.

Remarkably, during the first discharge, BMC exhibited a high capacity of 764 mAh g^{-1}. During the first charge, the VO_2 surface was covered by $Zn_x(OTf)_y(OH)_{2x-y}\cdot nH_2O$ (the product of H^+ insertion,[11] Figure S5) at 0.67 V and $Zn(OTf)_2$ at 0.69 V (Figure S6), suggesting the ~0.68 V platform was related to H^+ extraction and thus the O1/R1 peaks in Figure 1a could be attributed to H^+ storage. Note that the O2/R2 and O3/R3 peaks in BMC (Figure 1a) are consistent with Ji's research,[12] which can also be attributed to H^+ storage. During the next cycle, the much higher reversible capacity of the BMC (540 mAh g^{-1}) than the GFC (305 mAh g^{-1}) can be attributed to enhanced H^+ storage (Figure 1c). Moreover, the two elongations in the charge/discharge curves of BMC compared to GFC correspond to the additional O1/R1 and O3/R3 peaks in Figure 1a compared to Figure 1b. Interestingly, the in situ XRD patterns showed that the VO_2 (401) and (112) peaks have almost no shift during cycling of the BMC (Figure S8). As H^+ insertion led to lattice expansion and Zn^{2+} insertion led to lattice contraction,[5] the enhanced H^+ insertion in the BMC can be matched with a large amount Zn^{2+} insertion to thus maintain a more stable VO_2 lattice during cycling.

On the other hand, the OH^- generated by the BM was selectively transported to the anode chamber. Note that the Zn anode was clinging to the BM separator, such that the generated OH^- would immediately participate in reaction (1):

$$Zn^{2+} + ay/2Zn(OTf)_2 + 2OH^- + anH_2O \leftrightarrow aZn_x(OTf)_y(OH)_{2x-y}\cdot nH_2O \quad (1)$$

$$(a(2x-y) = 2) \quad (2)$$

$$Zn^{2+} + 2e^- \leftrightarrow Zn \quad (3)$$

From the above equations, the Zn platting/stripping (as well as the formation of zinc dendrite) is accompanied by the formation of $Zn_x(OTf)_y(OH)_{2x-y}\cdot nH_2O$ on the battery's anode in the BMC. Therefore, the zinc surface is covered by $Zn_x(OTf)_y(OH)_{2x-y}\cdot nH_2O$ uniformly after cycling (Figure S10). Comparing SEM images in Figure 2b,c to Figure 2a, the $Zn_x(OTf)_y(OH)_{2x-y}\cdot nH_2O$ is distributed smoothly and few zinc dendrite

https://dx.doi.org/10.1021/acsenergylett.0c02683
ACS Energy Lett. 2021, 6, 684−686

hotspots are observed. The sectional view also represents the regions of dispersed zinc dendrites, revealing that zinc dendrites pierce the $Zn_x(OTf)_y(OH)_{2x-y}\cdot nH_2O$ layer slightly but their growth is inhibited. Zinc dendrites are thicker in the BMC (~40 μm) than in the GFM (~15 μm), indicating that the surface $Zn_x(OTf)_y(OH)_{2x-y}\cdot nH_2O$ suppresses zinc dendrite growth. Moreover, Zn anodes after cycling in BMC and GFC present a silver gray and bright silver luster, respectively, corresponding to the uniformly distributed $Zn_x(OTf)_y(OH)_{2x-y}\cdot nH_2O$ and severe zinc dendrites (optical images in Figure 2b,c).

As the stability of the cathode and anode are both enhanced, we achieved an ultra-long cycling performance. The capacity of GFC decays rapidly and remains at ~20 mAh g^{-1} after 650 cycles due to the destruction of the cathode host caused by Zn^{2+} divalent chemistry and the severe zinc dendrites, while BMC retains a capacity of 50 mAh g^{-1} even after long-term cycling of 4500 cycles, corresponding to a running time of ~4440 h (Figure 2d). Figure S11 exhibits the conformal charge/discharge curves for the 3000th, 4000th, and 4500th cycles of BMC, indicating the nearly unaltered electrochemistry after cycling. Note that in most cases, AZIBs can be operated steadily for a short time of less than 100 cycles under deep charging/discharging conditions.[13−15]

In conclusion, we surprisingly achieved an ultra-long running time of ~4440 h for AZIBs through generating H^+ in the catholyte and OH^- in the anolyte via BM separators. Further development and comprehension of the bipolar separators will be significant in the future.

■ ASSOCIATED CONTENT

Supporting Information

The Supporting Information is available free of charge at https://pubs.acs.org/doi/10.1021/acsenergylett.0c02683.

Experimental details and characterization data (PDF)

■ AUTHOR INFORMATION

Corresponding Authors

Lei Zhang − *Department of Physical Science and Technology, School of Science, Wuhan University of Technology, Wuhan 430070, China*; Email: Z1016149568@163.com

Liqiang Mai − *State Key Laboratory of Advanced Technology for Materials Synthesis and Processing, Wuhan University of Technology, Wuhan 430070, China*; orcid.org/0000-0003-4259-7725; Email: mlq518@whut.edu.cn

Authors

Yuhang Dai − *State Key Laboratory of Advanced Technology for Materials Synthesis and Processing, Wuhan University of Technology, Wuhan 430070, China*

Jinghao Li − *State Key Laboratory of Advanced Technology for Materials Synthesis and Processing, Wuhan University of Technology, Wuhan 430070, China*

Lineng Chen − *State Key Laboratory of Advanced Technology for Materials Synthesis and Processing, Wuhan University of Technology, Wuhan 430070, China*

Kehan Le − *State Key Laboratory of Advanced Technology for Materials Synthesis and Processing, Wuhan University of Technology, Wuhan 430070, China*

Zhijun Cai − *State Key Laboratory of Advanced Technology for Materials Synthesis and Processing, Wuhan University of Technology, Wuhan 430070, China*

Qinyou An − *State Key Laboratory of Advanced Technology for Materials Synthesis and Processing, Wuhan University of Technology, Wuhan 430070, China*; orcid.org/0000-0003-0605-4942

Complete contact information is available at: https://pubs.acs.org/10.1021/acsenergylett.0c02683

Author Contributions

#Y.D. and J.L. contributed equally to this work.

Notes

The authors declare no competing financial interest.

■ ACKNOWLEDGMENTS

This research was supported by the National Key Research and Development Program of China (2020YFA0715000, 2018FYB-0104202, 2016YFA0202603), the National Natural Science Foundation of China (51832004, 51521001), and the Program of Introducing Talents of Discipline to Universities (B17034).

■ REFERENCES

(1) Jacoby, M. Safer Lithium-Ion Batteries. *Chem. Eng. News* **2013**, *91* (6), 33−37.

(2) Roth, E. P.; Orendorff, C. J. How Electrolytes Influence Battery Safety. *Electrochem. Soc. Interface* **2012**, *21*, 45−49.

(3) Wanger, T. C. The Lithium Future-Resources, Recycling, and the Environment. *Conserv. Lett.* **2011**, *4*, 202−206.

(4) Fang, G.; Zhou, J.; Pan, A.; Liang, S. Recent Advances in Aqueous Zinc-Ion Batteries. *ACS Energy Lett.* **2018**, *3*, 2480−2501.

(5) Wang, L.; Huang, K. W.; Chen, J.; Zheng, J. Ultralong Cycle Stability of Aqueous Zinc-Ion Batteries with Zinc Vanadium Oxide Cathodes. *Sci. Adv.* **2019**, *5*, eaax4279.

(6) Naveed, A.; Yang, H.; Shao, Y.; Yang, J.; Yanna, N.; Liu, J.; Shi, S.; Zhang, L.; Ye, A.; He, B.; Wang, J. A Highly Reversible Zn Anode with Intrinsically Safe Organic Electrolyte for Long-Cycle-Life Batteries. *Adv. Mater.* **2019**, *31*, 1900668.

(7) Wang, F.; Borodin, O.; Gao, T.; Fan, X.; Sun, W.; Han, F.; Faraone, A.; Dura, J. A.; Xu, K.; Wang, C. Highly Reversible Zinc Metal Anode for Aqueous Batteries. *Nat. Mater.* **2018**, *17*, 543−549.

(8) Zhang, N.; Chen, X.; Yu, M.; Niu, Z.; Cheng, F.; Chen, J. Materials Chemistry for Rechargeable Zinc-Ion Batteries. *Chem. Soc. Rev.* **2020**, *49*, 4203−4219.

(9) Zhong, C.; Liu, B.; Ding, J.; Liu, X.; Zhong, Y.; Li, Y.; Sun, C.; Han, X.; Deng, Y.; Zhao, N.; Hu, W. Decoupling Electrolytes towards Stable and High-Energy Rechargeable Aqueous Zinc−Manganese Dioxide Batteries. *Nat. Energy* **2020**, *5*, 440−449.

(10) Wei, T.; Li, Q.; Yang, G.; Wang, C. An Electrochemically Induced Bilayered Structure Facilitates Long-Life Zinc Storage of Vanadium Dioxide. *J. Mater. Chem. A* **2018**, *6*, 8006−8012.

(11) Oberholzer, P.; Tervoort, E.; Bouzid, A.; Pasquarello, A.; Kundu, D. Oxide versus Nonoxide Cathode Materials for Aqueous Zn Batteries: An Insight into the Charge Storage Mechanism and Consequences Thereof. *ACS Appl. Mater. Interfaces* **2019**, *11*, 674−682.

(12) Wu, X.; Hong, J. J.; Shin, W.; Ma, L.; Liu, T.; Bi, X.; Yuan, Y.; Qi, Y.; Surta, T. W.; Huang, W.; Neuefeind, J.; Wu, T.; Greaney, P. A.; Lu, J.; Ji, X. Diffusion-Free Grotthuss Topochemistry for High-Rate and Long-Life Proton Batteries. *Nat. Energy* **2019**, *4*, 123−130.

(13) Pan, H.; Shao, Y.; Yan, P.; Cheng, Y.; Han, K. S.; Nie, Z.; Wang, C.; Yang, J.; Li, X.; Bhattacharya, P.; Mueller, K. T.; Liu, J. Reversible Aqueous Zinc/Manganese Oxide Energy Storage from Conversion Reactions. *Nat. Energy* **2016**, *1*, 16039.

(14) Kundu, D.; Adams, B. D.; Duffort, V.; Vajargah, S. H.; Nazar, L. F. A High-Capacity and Long-Life Aqueous Rechargeable Zinc Battery Using a Metal Oxide Intercalation Cathode. *Nat. Energy* **2016**, *1*, 16119.

(15) Chen, L.; Ruan, Y.; Zhang, G.; Wei, Q.; Jiang, Y.; Xiong, T.; He, P.; Yang, W.; Yan, M.; An, Q.; Mai, L. Ultrastable and High-Performance Zn/VO_2 Battery Based on a Reversible Single-Phase Reaction. *Chem. Mater.* **2019**, *31*, 699−706.